Modeling of a Micro-Machined Pulsed Plasma Thruster

IEPC-2005-043

Presented at the 29th International Electric Propulsion Conference, Princeton University, October 31 – November 4, 2005

Michael Keidar* and Iain D. Boyd†
University of Michigan, Ann Arbor MI

Daniel Simon‡ and Bohdan Cybyk §
The Johns Hopkins University Applied Physics Laboratory, Laurel, MD

Abstract: In this paper we summarize some recent analysis of a micro-PPT developed at JHU/APL. The analysis involves modeling of the Teflon ablation, plasma generation, and acceleration in the vicinity of the propellant. The Teflon ablation model is based on a kinetic ablation model for a micro-PPT. The plasma energy balance and heat transfer to the Teflon is based on a previously developed model for a micro-PPT. In the transitional region between the plasma and ablated surface, two different layers can be distinguished, namely a kinetic non-equilibrium layer adjacent to the ablating surface and a collisional non-equilibrium layer with ionization and thermal non-equilibrium. The coupled solution between these two layers yields the ablation rate. It is found that the ablation rate decreases with electrode width. Both equilibrium and non-equilibrium ionization mechanisms are considered and the parameter range for applicability of these mechanisms is established. The plasma acceleration study concludes that specific impulse decreases with an increasing interelectrode gap. In addition we present some preliminary results for the near field plume. It is shown that due to the highly collisonal nature of the plasma at the thruster ext, some carbon atoms are scattered into the backflow region.

I. Introduction

The pulsed plasma thruster (PPT) concept is an electric propulsion device that lends itself well towards miniaturization. These thrusters essentially consist of two parallel electrodes connected to a high voltage capacitor. Electrical discharges between the electrodes ionize and accelerate propellant via a combination of gasdynamic and electromagnetic forces. The electrodes in conventional scale PPTs are typically spaced several centimeters apart and operate at a potential difference of 1000 Volts or more.

Several miniature varieties of pulsed plasma thruster have been successful developed at tested by researchers at The Johns Hopkins University Applied Physics Laboratory (JHU/APL). A 2-D solid propellant version consumes several alternating layers of Teflon and copper embedded within a fiberglass or ceramic substrate. A 2-D liquid propellant version is fabricated from a fiberglass substrate and can utilize any number of liquefied propellants, including water, ammonia, and hydrazine[1]. Both versions are incredibly compact and contain no moving parts.

* Research Scientist, Department of Aerospace Engineering, keidar@umich.edu.
† Professor, Department of Aerospace Engineering.
‡ Aerospace Engineer, Research & Technology Development Center
§ Aerospace Engineer, Research & Technology Development Center

Furthermore, their minuscule electrode gap spacings (380–1000 mm) allow them to operate at moderate voltages (250–600 Volts) and utilize miniature power processing circuits.

In this document we summarize analysis of the solid propellant (Teflon-based) micro-PPT developed at JHU/APL. We start from analysis of the Teflon ablation, plasma generation and acceleration in the vicinity of propellant. In addition we present some preliminary results for the near-field plume.

II. Model of the plasma layer in the case an ablative micro-PPT

In this section we briefly describe the development of a model for the plasma layer near the evaporating surface with application to a JHU/APL micro-PPT. This model includes the following features: Teflon ablation, plasma energy balance, heat transfer from the plasma to the Teflon, and current distribution. The Teflon ablation is based on a kinetic ablation model for the micro-PPT (Refs. 2,3,4). The plasma energy balance and heat transfer to the Teflon is based on a previously develop model for a micro-PPT.[2,3] The energy balance can be written in the following form:

$$\frac{3}{2} n \frac{dT_e}{dt} = Q_j - Q_{rad} - Q_{flux} \qquad (1)$$

where n is the plasma density, T_e is the electron temperature, Q_j is the Joule heating, Q_{rad} is the radiation heat and Q_{flux} is the energy flux due to particle convection. The Joule heat term is equal to $Q_j=j^2/\sigma$, where $\sigma=e^2n/(\nu_{ei}m_e)$; $\nu_{ei} = \frac{\ln \Lambda Z_i n}{3\cdot 10^{10} T_e^{3/2}}$ (Ref. [5]). One can see that the plasma conductivity has only a weak dependence on the plasma density (in the Coulomb logarithm). The radiation heat flux Q_{rad} and particle convection heat flux Q_{flux} depend on the plasma density and temperature. According to Ref.6, the radiation in continuum from a C-F plasma in the considered parameter range (n=10^{22}-10^{24} m^{-3}, T_e=1-3 eV) provides the main contribution. The radiation energy flux Q_{rad} includes the radiation for a continuum spectrum based on a theoretical model.[7,8] The radiation term calculation is described in detail elsewhere.[8-10,14] The particle convection flux Q_{flux} includes energy associated with electron and ion fluxes to the Teflon™. In the steady-state (floating potential) the ion and electron particle flux to the surface can be calculated as follows: $j_i(2T_e + U_{sh} + T_e)$. Electron temperature is assumed to be constant across the plasma layer due to large electron thermal conductivity.[9] More details about the model and computational methods can be found elsewhere.[10]

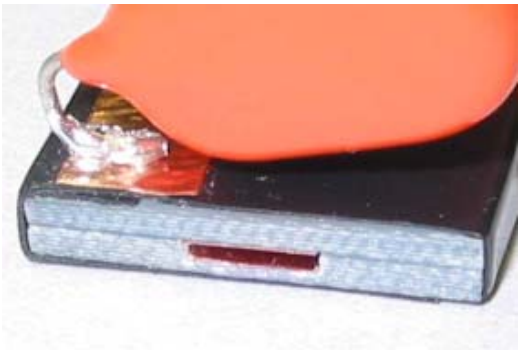

Fig 1a. Exit plane of ablative micro-PPT.

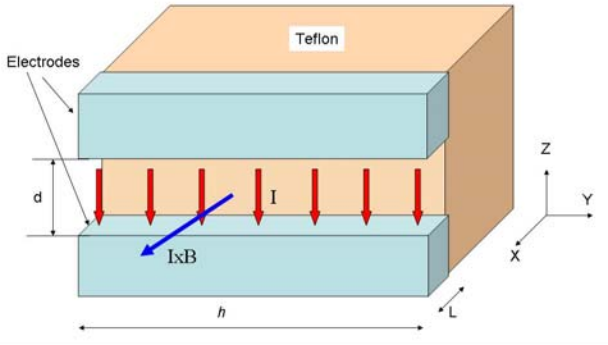

Fig 1b. Schematic of thruster model geometry.

The thruster hardware and schematic are shown in Fig.1. Two geometrical parameters are important for our consideration, namely electrode length *L* and electrode width *h*. We start from a brief summary of the ablation model. In the transitional region between the plasma and ablated surface, two different layers can be distinguished, namely a kinetic non-equilibrium layer adjacent to the ablated surface and a collisional non-equilibrium layer with ionization and thermal non-equilibrium. The coupling solution between these two layers yields the ablation rate. Similarly to the previous works, we consider the multi-layer structure of the near surface region (see Fig. 2). There are two different characteristic layers between the surface and the plasma bulk: (1) a kinetic non-equilibrium layer adjacent to the surface with a thickness of a few mean free paths (the Knudsen layer), (2) a collision-dominated (hydrodynamic) layer. To simplify the present analysis, we assume that ionization equilibrium is reached near the edge of the second layer between boundaries 1 and 2. Therefore, the electron density at boundary 2 will be calculated using Saha equilibrium. Solution of the hydrodynamic layer problem depends on the boundary conditions at boundary 1, which is the Knudsen layer edge. To find the parameters at the edge of the Knudsen layer as a function of velocity at the Knudsen layer edge, V_1, we apply the mass, momentum and energy conservation equations in kinetic form. Corresponding relations between parameters at the edge of the Knudsen layer and those at the surface were presented elsewhere[11]. From the hydrodynamic equations one can readily obtain the velocity at the edge of the Knudsen layer:

$$V_1^2 = \frac{2kT_1}{m} \cdot \frac{\frac{n_1}{2} - \frac{T_2 n_2}{2T_1}}{\frac{3}{2} \cdot \frac{n_1^2}{n_2} - n_1} \qquad (2)$$

The velocity V_1 as well as density n_1 determine the ablation rate: $\Gamma = m n_1 V_1$, where m is the heavy particle mass. It was shown[9] that the velocity V_1 increases with discharge energy and approaches its maximum value of the local sonic speed (as happens in the case of ablation into vacuum) for a certain energy. This happens because stronger plasma acceleration leads to conditions close to the expansion into vacuum. It is expected that this effect should affect the ablation rate, since ablation rate is directly proportional to the velocity at the Knudsen layer edge.

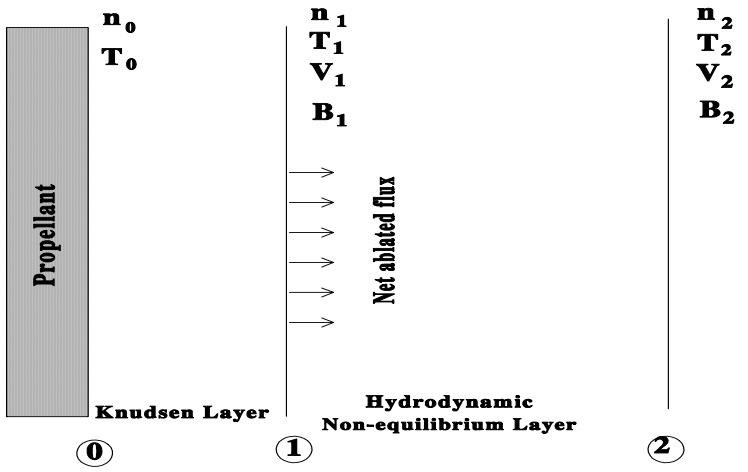

Fig 2. Schematic of the multi-layer structure near the propellant face in a micro-PPT.

The plasma layer model is combined with the heat conductivity model in the Teflon. The temperature can be calculated from the heat transfer equation:

$$\frac{\partial T}{\partial t} = a\Delta T \tag{3}$$

where $a=\lambda/C_p\rho$. Equation 3 is subject to the following boundary conditions at the propellant wall:

$$\begin{aligned} &-\lambda\partial T/\partial z(z=0) = q(t) - \Delta H\cdot\Gamma - C_p(T_s-T_o)\,\Gamma \\ &\lambda\partial T/\partial z(z=\infty) = 0 \\ &T(t=0)=T_o \end{aligned} \tag{4}$$

where z=0 corresponds to the dielectric surface and $q(t)$ is the density of the heat flux, consisting of the radiative and particle convection fluxes, determined according to Eq. 1. The radiation transport inside the solid Teflon was neglected in this analysis. Assuming that the thermal conductivity of the Teflon is small, we can reduce Eqs. (3,4) to a 1D problem and therefore we will solve the local heat balance problem instead of 2D heat balance over the electrode surface. After the surface temperature reaches some critical temperature, material sublimation begins and

ablation heat becomes significant in the energy balance. Under above conditions the temperature profile for the ablated Teflon is exponential:

$$T(z) = T_s exp(- z\Gamma C_p/\lambda) \qquad (5)$$

This system of equations determines the plasma parameter distribution in the vicinity of the ablated propellant.

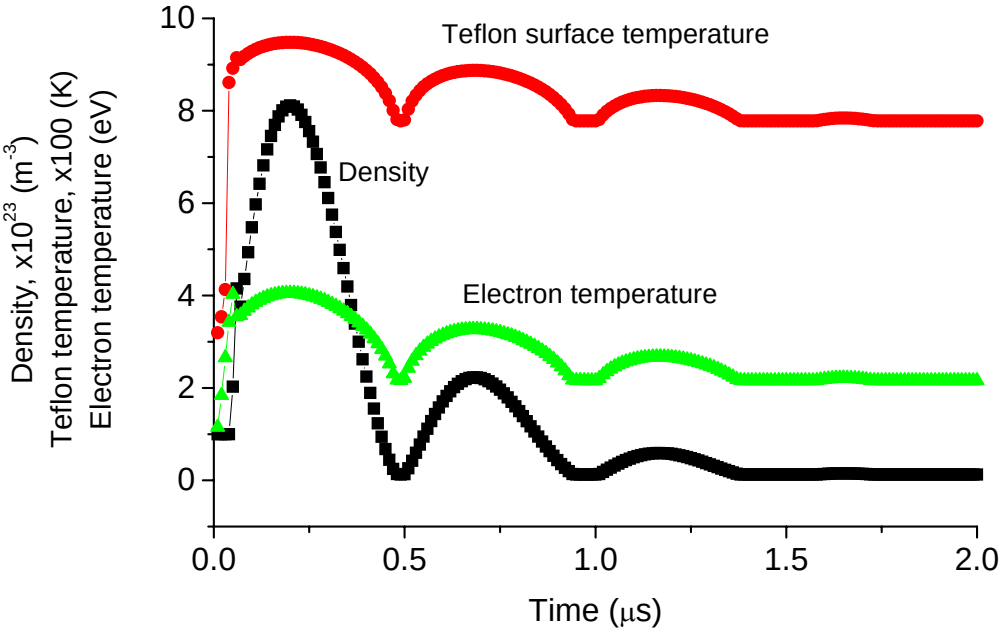

Fig 3. Plasma parameters during discharge (h=5 mm, d=990 μm, C=850 nF).

The calculated parameter distributions during typical discharge conditions are shown in Fig. 3. One can see that the Teflon surface temperature peaks at about 950 K. The electron temperature peaks at about 4 eV, while the plasma density is about $8 \cdot 10^{23}$ m^{-3}. Plasma parameter peaks correspond to the discharge current peak.

It was found that plasma parameters depend on the electrode width, *h*. For instance, in the case of *h*=2 mm the plasma parameter distribution is shown in Fig. 4. It can be seen that in this case Teflon surface temperature, electron temperature and plasma density significantly increase. As a result the ablated mass also increases with *h* decrease, due to high energy flux to the Teflon as shown in Fig.5.

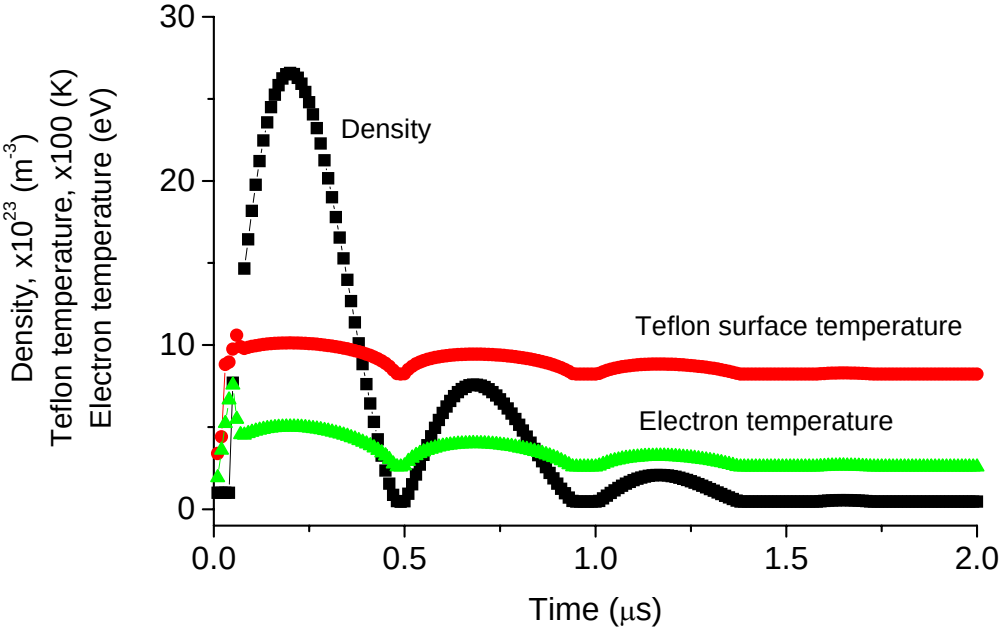

Fig 4. Plasma parameters during discharge (h=2 mm, d=990 μm, C=850 nF).

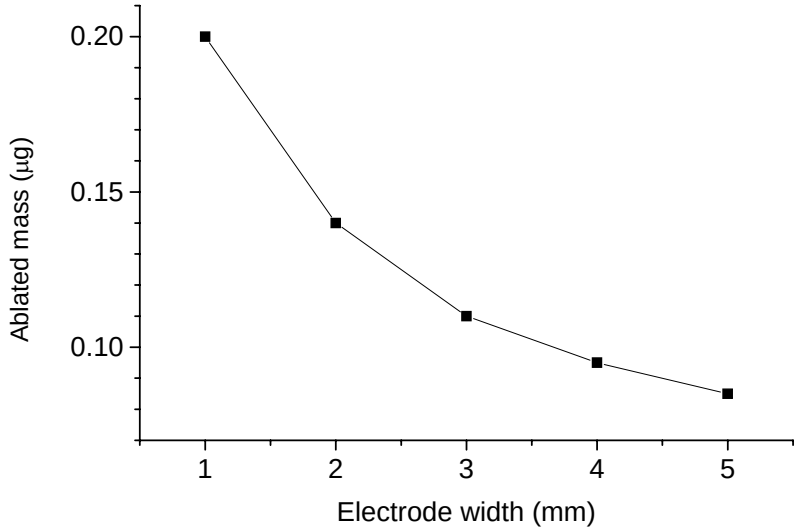

Fig 5. Dependence of the ablated mass on electrode width, *h*.

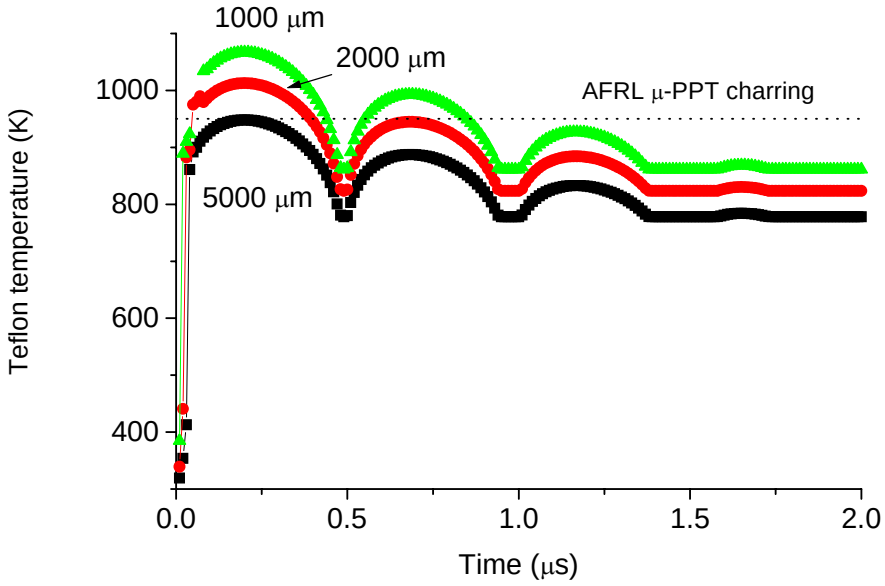

Fig 6. Teflon surface temperature with electrode width, *h*, as a parameter. Dotted line shows surface temperature limit for AFRL micro-PPT charring. According to the model everything above this line will not be charred.

It is important to note that Teflon surface temperature is very important in preventing surface charring or carbonization.[12] Higher surface temperature leads to higher ablation rate and as thus prevents the carbonization which is caused by the backflux of the Carbon ions and atoms from the plasma. According to previous study of the AFRL micro-PPT it was found that a surface temperature higher than 960 K guarantees the absence of the carbonization. In our analysis of the JHU/APL micro-PPT we found that electrode width significantly affects the surface temperature. According to these predictions if electrode width, h<2 mm one can expect that charring will be insignificant during the entire pulse as shown in Fig. 6.

III. Ionization study in micro-PPT

In this section we describe ionization analysis of the Teflon micro-PPT. The established way to investigate ionization state in micro-PPT is used.[9] In the Teflon surface temperature-electron temperature (T_s-T_e) plane, these dependencies are shown in Fig. 7. These dependencies were calculated using the micro-PPT model described in the previous section. On the other hand the separation curve between regimes with equilibrium and without equilibrium can be calculated using the non-equilibrium model described in detail in Ref. 9. It can be seen that in general both regimes with ionization equilibrium and without it can be achieved in the considered range of parameters. One can see that the separation curve depends upon the total current in the discharge. It follows from comparison that during the discharge there are regimes where equilibrium cannot be achieved. Therefore, the plasma composition in the

plasma layer cannot always be calculated based on LTE assumption but rather the more general model (as described in Ref. 9) should be employed.

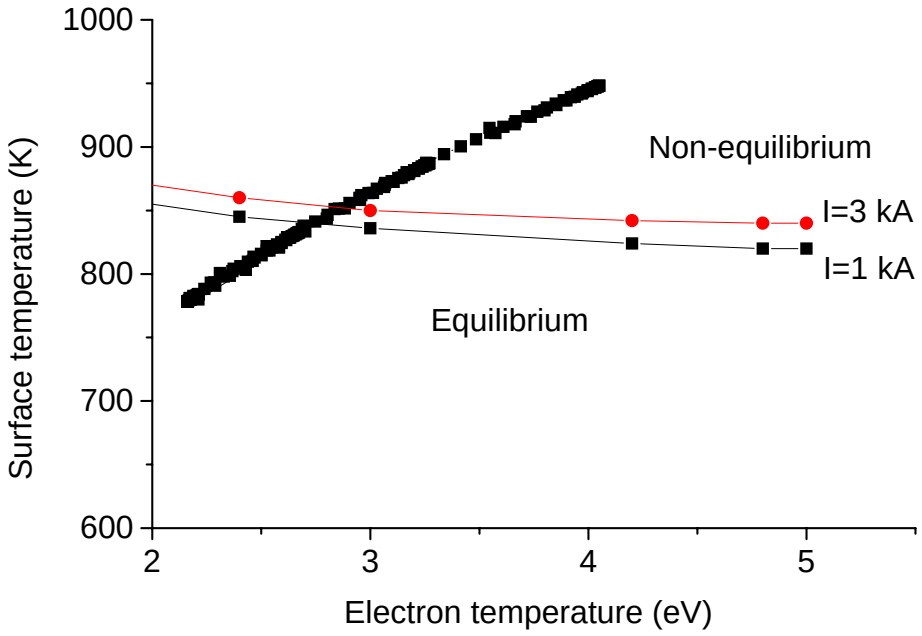

Fig 7. Surface temperature-electron temperature plane. Division between parameter range for equilibrium and non-equilibrium ionization conditions

IV. Model of the acceleration region

In order to calculate the current density in the thruster channel we assume that the magnetic field has only a *y* component and we also neglect the displacement current. The main plasma density gradient developed in the axial direction and therefore gradient mechanism[13] should not affect magnetic transport in this system. The combination of the Maxwell equations and electron momentum conservation gives the following equation for the magnetic field in the case of isothermal flow:

$$\partial \mathbf{B}/\partial t = 1/(\sigma\mu)\nabla^2\mathbf{B} - \nabla\times(\mathbf{j}\times\mathbf{B}/(en_e)) + \nabla\times(\mathbf{V}\times\mathbf{B}) \qquad (6)$$

A scaling analysis shows that the various terms on the right hand side of Eq. 6 may have importance in different regions of the plasma plume and therefore a general end-to-end plasma plume analysis requires keeping all terms in the equation. In the case of the near plume of the micro-PPT with a characteristic scale length of about 1 cm, the magnetic Reynolds number $Re_m << 1$ and therefore the last term can be neglected. In addition our estimations show that the Hall parameter $(\omega\tau) << 1$ if the plasma density near the Teflon surface $n_e > 10^{23}$ m^{-3}. This case is realized in

the micro-PPT so the Hall effect is expected to be small for this particular case. Therefore all results presented below are calculated from a simple magnetic diffusion equation without considering the Hall effect, i.e. the second term in the right side hand of Eq. 6 can also be neglected. The plasma dynamics is described by the following system of equations:

$$\frac{\partial \rho}{\partial t} + \frac{\partial (\rho V)}{\partial x} = 0 \tag{7}$$

$$\rho\left(\frac{\partial V}{\partial t} + V\frac{\partial V}{\partial x}\right) = -\frac{\partial P}{\partial x} - (j \times B) \tag{8}$$

The boundary condition is that the magnetosonic condition is developed at the thruster exit plane. In other words, this assumption is equivalent to the condition that most of the plasma acceleration takes place in the interelectrode region:

$$V_A = \frac{B}{(\mu n M)^{0.5}} \tag{9}$$

where n is the electron density at the exit plane. To close the system of equations for the hydrodynamic layer, and taking into account that the magnetic field decreases along the channel, we can estimate the magnetic field at the edge of the Knudsen layer (boundary 1, see Fig.2) as:

$$B_o = \mu \cdot I/h \tag{10}$$

The velocity distribution along the thruster channel is shown in Fig.8. One can see that velocity increases towards the exit plane due to electromagnetic acceleration, which is higher when discharge current has peaks. The maximum velocity is about 3 sound speeds (based on electron temperature) in the case of h=5 mm. The density distribution is shown in Fig. 9. It can be seen that the density decreases due to acceleration.

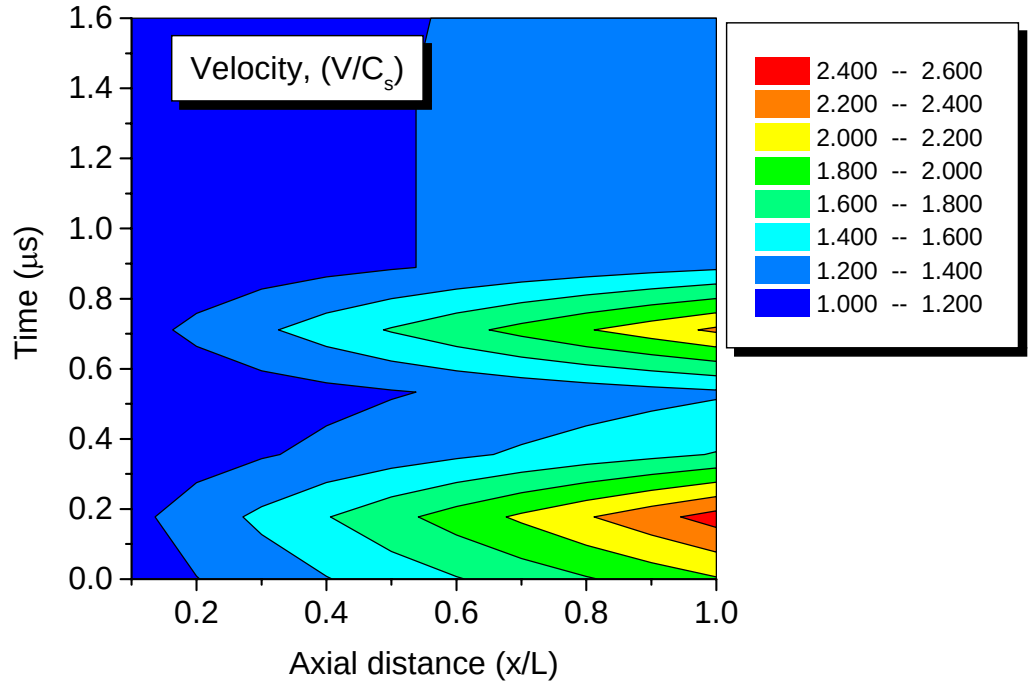

Fig 8. Velocity distribution in the micro-PPT channel (h=5 mm, d=990 μm, C=850 nF).

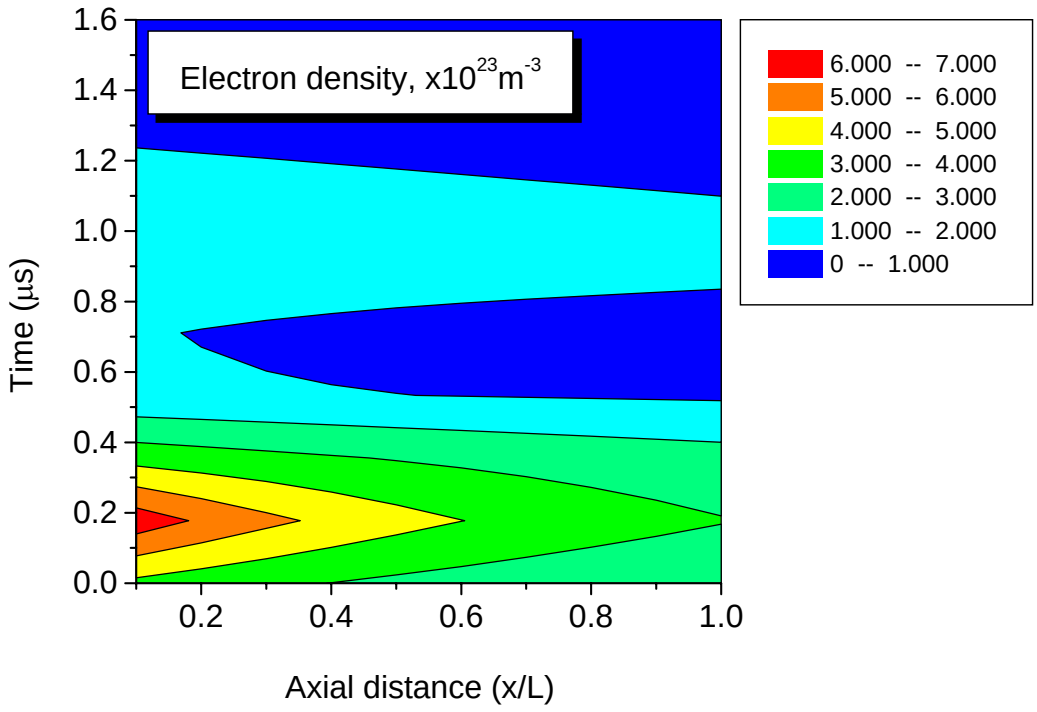

Fig 9. Density distribution in micro-PPT channel (h=5 mm, d=990 μm, C=850 nF).

It was found that the thruster geometry significantly affects acceleration in the micro-PPT as shown in Fig.10. One can see that velocity at the thruster exit plane increases with interelectrode gap decrease for a given discharge current. Thus according to this model prediction, a thruster with a smaller interelectrode gap will produce large exit velocity and therefore larger specific impulse.

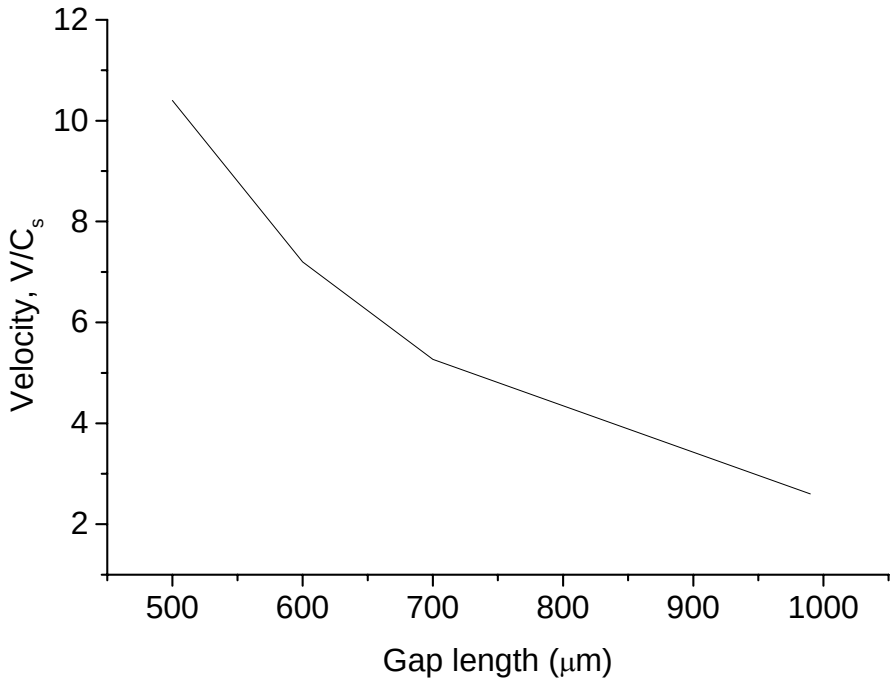

Fig 10. Dependence of the velocity on the interelectrode gap length, *d*.

V. Plume simulation

The boundary conditions generated at the thruster exit following the approaches described above are shown in Figs. 11a and 11b. Due to the high specific power of this device, ions dominate over atoms and fluorine composition is about double that for carbon, since Teflon has composition C_2F_4. These profiles are used as starting conditions in our existing DSMC-PIC PPT plume code[14] to model the plume of the APL micro-PPT in an axially symmetric coordinate frame.

In the present work, we employ a hybrid particle-fluid approach. Neutrals (C and F) and ions (C+ and F+) are modeled as particles. Particle collisions are computed using the direct simulation Monte Carlo method (DSMC).[15] Both momentum exchange and charge exchange collisions are simulated. Momentum exchange cross sections employ the model of Dalgarno et al. [16] and the collision dynamics follows the usual DSMC procedures. The charge exchange processes employ the cross sections proposed by Sakabe and Izawa.[17] Acceleration of the charged particles in self-consistent electric fields is simulated using the Particle-In-Cell method (PIC)[18]. The plasma

potential, φ, is obtained by assuming charge neutrality to determine the electron number density from the total ion density. The electron number density, n_e, is then used in the Boltzmann relation to obtain the plasma potential:

$$\varphi = T_e(t) \ln\left(\frac{n_e}{n_{ref}(t)} \right) \tag{11}$$

where the electron temperature, T_e (t), is in electron volts and n_{ref} (t) is the electron number density at a reference point. Both of these quantities vary in time throughout the pulse and are set to the plasma temperature and number density at the thruster exit that are obtained from the thruster simulation. It is assumed that the potential here is constant at zero.

Since charge neutrality is assumed, the PIC cells do not need to be of the order of the Debye length. Instead they are chosen to be small enough to resolve in a reasonable way the gradients in the potential. For DSMC, the grids should be scaled according to the local mean free path, but this is not possible in the present work due to the very large plasma density. The grids employed in the computation are shown in Fig.12. A single time-step given by the reciprocal of the maximum plasma frequency is employed throughout. All results are time-dependent and are integrated over small intervals of 0.25 μsec. The maximum number of particles in the simulation exceeds 3.5 million and the total computation time is about one day.

The main difficulties in performing the computations of the PPT plume arise from the transient nature of the expansion. There are often regions of the flow where the number of simulated particles is very small. This occurs at the leading edge of the forward expansion at early times, and at the trailing edge of the expansion at late times. The low number of particles in these regions leads to significant scatter in the simulation results in these regions.

Particles are introduced into the flow field through the thruster exit plane using the output from the plasma generation model (Fig. 11). The particular example is a micro-PPT with the following geometry: electrode width h=5 mm, interelectrode gap d=990 micron, electrode length L=600 microns (see Fig.1). A uniform radial profile of properties is assumed across the exit plane. Ions and neutrals are assumed to have the same velocity and the same temperature. This assumption is based on the fact that the number densities are relatively high so that the frequency of charge exchange collisions inside the nozzle is high. Simulations are performed without any facility back pressure.

To illustrate some of the basic dynamics of the time evolution of the PPT plume expansion processes, contours of carbon ion number density are shown at four different times in Figs. 13a-13d. These plots clearly illustrate how ions are pushed into the backflow region through the collision and electric field processes. To demonstrate the different dynamics of ions and neutrals, carbon atom number density contours are shown at four different times in Figs. 14a-

14d. Due to the highly collisional nature of the plasma at the thruster exit, some carbon atoms are also scattered into the backflow region.

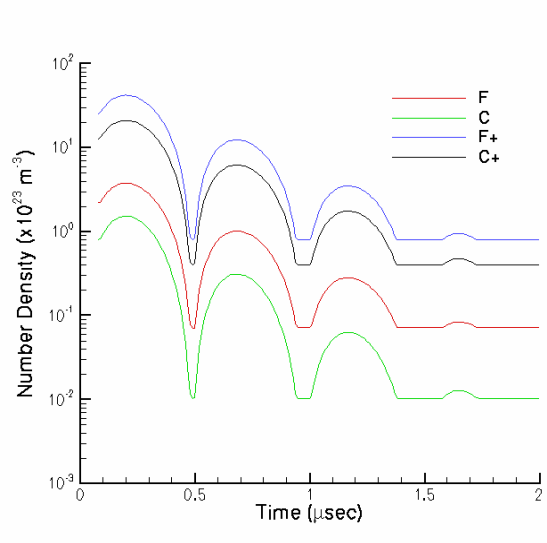

Fig 11a. Temporal thruster exit conditions.

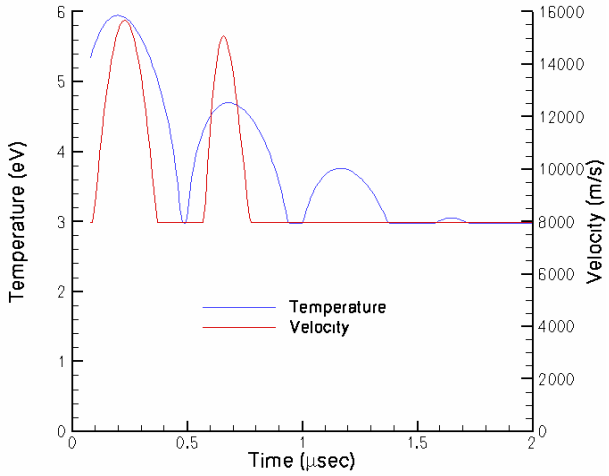

Fig 11b. Temporal thruster exit conditions.

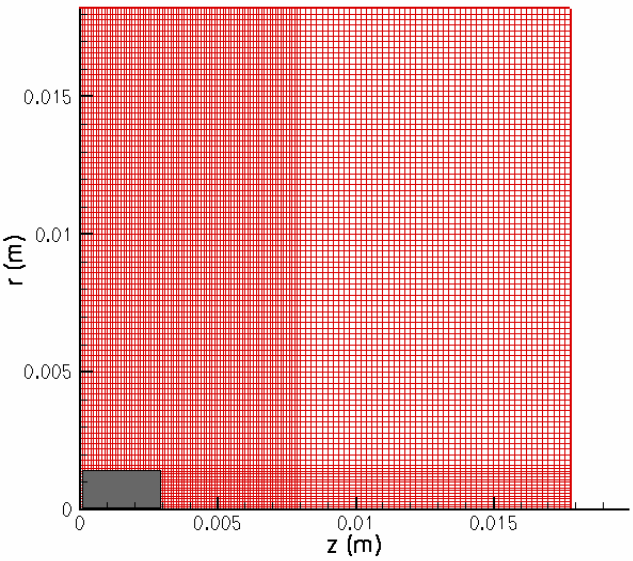

Fig 12. Computational domain.

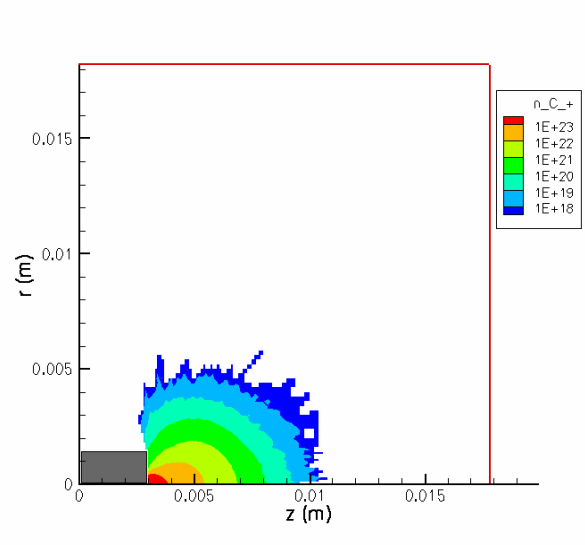

Fig 13a. Carbon ion density at 0.33µsec.

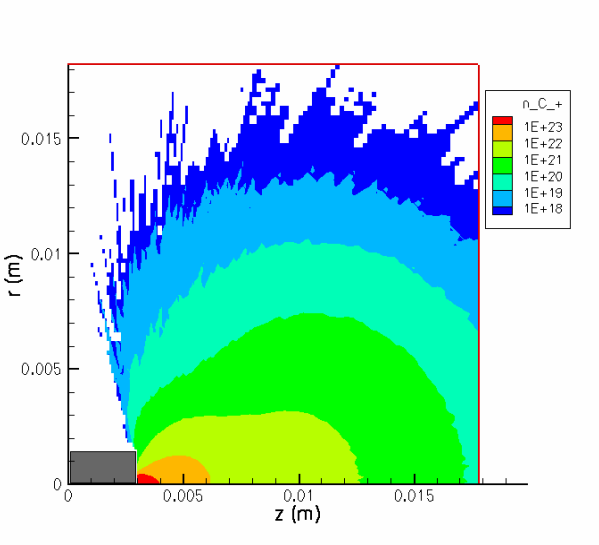

Fig 13b. Carbon ion density at 0.83µsec.

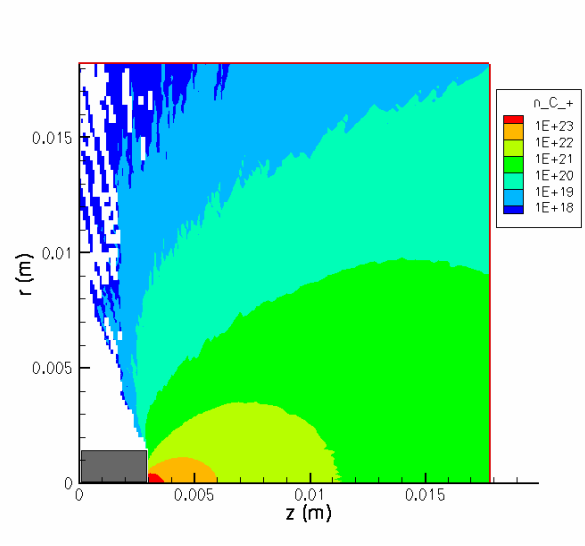

Fig 13c. Carbon ion density at 1.58µsec.

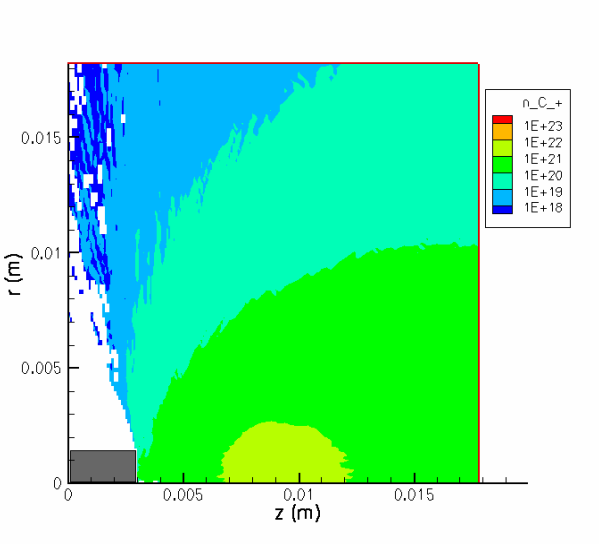

Fig 13d. Carbon ion density at 2.58µsec.

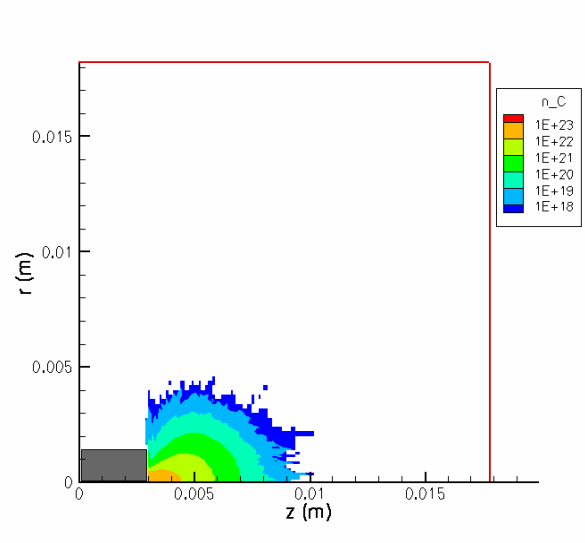

Fig 14a. Carbon atom density at 0.33μsec.

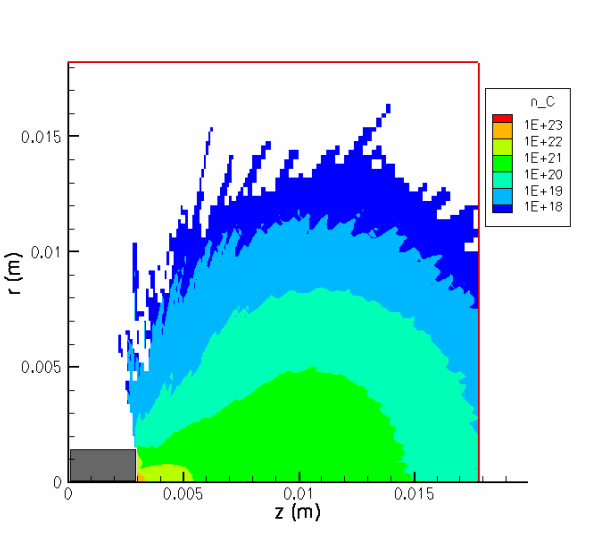

Fig 14b. Carbon atom density at 0.83μsec.

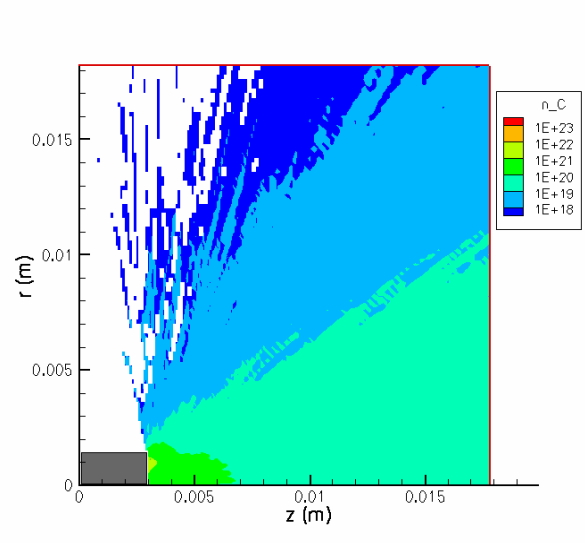

Fig 14c. Carbon atom density at 1.58μsec.

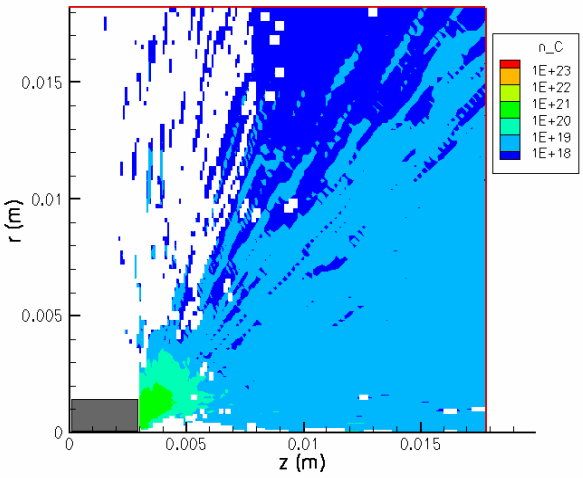

Fig 14d. Carbon atom density at 2.58μsec.

VI. Concluding remarks

The analysis of the JHU/APL micro-PPT presented in this paper involved modeling of the Teflon ablation, plasma generation and acceleration in the vicinity of propellant. The Teflon ablation model was based on a kinetic ablation model for a micro-PPT. According to this model in the transitional region between the plasma and ablated surface, two different layers can be distinguished, namely a kinetic non-equilibrium layer adjacent to the ablating surface and a collisional non-equilibrium layer with ionization and thermal non-equilibrium. The coupled solution between these two layers yields the ablation rate.

According to model prediction the Teflon surface temperature peaks at about 950 K, the electron temperature peaks at about 4 eV, while the plasma density is about $8 \cdot 10^{23}$ m^{-3} in the case of micro-PPT having electrode width of about 5 mm. Surface temperature increases with electrode width decrease. In turn, higher surface temperature leads to higher ablation rate and as thus prevents the carbonization, which is caused by the backflux of the carbon ions and atoms from the plasma. According to previous study of the AFRL micro-PPT it was found that a surface temperature higher than 960 K guarantees the absence of the carbonization. According to these predictions if electrode width is less than 2 mm one can expect that charring will be insignificant during the entire pulse. In addition it was found that the thruster geometry significantly affects acceleration, so that a thruster with a smaller interelectrode gap will produce large exit velocity and therefore larger specific impulse.

In addition some preliminary results for the near field plume were presented. It was shown that ions are pushed into the backflow region through the collision and electric field processes. Due to the highly collisional nature of the plasma at the thruster exit, some carbon atoms are also scattered into the backflow region.

References

[1] D. Simon and B. Land, Micro Pulsed Plasma Thruster Technology Development, *40th AIAA Joint Propulsion Conference*, Fort Lauderdale, FL, USA, July 2004, Paper AIAA-2004-3622.

[2] M. Keidar, I.G. Boyd and I.I. Beilis, On the Model of Teflon ablation in ablation-controlled discharge, *J. Phys. D: Applied Physics*, 34, 2001, pp. 1675-1677.

[3] M. Keidar, I.D. Boyd, E. L. Antonsen and G. G. Spanjers, Progress in development of modeling capabilities for a micro-pulsed plasma thruster, *39th AIAA Joint Propulsion Conference*, Huntsville, AL, USA, July 2003, Paper AIAA-03-5166.

[4] M. Keidar and I. D. Boyd, Optimization issues for a micro-pulsed plasma thruster, *40th AIAA Joint Propulsion Conference*, Fort Lauderdale, FL, USA, July 2004, Paper AIAA-04-4119.

[5] S.I. Braginsky, in Review of Plasma Physics, Edited by M.A. Leontovich (Consultant Bureau, New York, 1965), Volume 1.

[6] A. I. Zemskov, V. V. Prut, and V. A. Khrabrov, "Pulsed Discharge in Dielectric Chamber", *Sov. Phys. Tech. Phys.*, 17, 1972, pp. 285-289.

[7] G. I. Kozlov, V. A. Kuznetsov, and V. A. Masyukov, "Radiative Losses by Argon Plasma and the Emissive Model of a Continuos Optical Discharge", *Sov. Phys. JETP*, 39, 1974, pp.463-468.

[8] Y. P. Raizer, Gas Discharge Physics, Moscow, Nauka, 1987

[9] M. Keidar, I.D. Boyd, and I.I. Beilis, "Ionization and ablation phenomena in an ablative plasma accelerator", *Journal of Applied Physics*, Vol. 96, No. 10, 2004, pp. 5420-5428.

[10] M. Keidar, I. D. Boyd, E. L. Antonsen and G.G. Spanjers, "Electromagnetic Effects in the Near Field Plume Exhaust of a Micro-Pulsed Plasma Thruster", *Journal of Propulsion & Power*, 2004, v. 20, No. 6, pp. 961-969.

[11] M. Keidar, J. Fan, I.D. Boyd and I.I. Beilis, "Vaporization of heated materials into discharge plasmas", *J. Appl. Phys*., 89, 2001, pp. 3095-3098.

[12] M. Keidar, I.D. Boyd, E.L. Antonsen, F.S. Gulczinski III and G.G. Spanjers, Propellant charring in pulsed plasma thrusters, *Journal Propulsion & Power*, 20, No. 6, 2004, pp. 978-984.

[13] A.S. Kingsep, Yu.V. Mokhov and K.V. Chukbar, Sov. J. Plasma Phys., 10(4) 1984 p. 495

[14] Boyd, I.D., Keidar, M. and McKeon, W., "Modeling of a Pulsed Plasma Thruster From Plasma Generation to Plume Far Field," *Journal of Spacecraft and Rockets*, Vol. 37, 2000, pp. 399-407.

[15] Bird, G.A., Molecular Gas Dynamics and the Direct Simulation of Gas Flows, Oxford University Press, 1994.

[16] Dalgarno, A., McDowell, M.R.C., and Williams, A., "The Mobilities of Ions in Unlike Gases," *Proceedings of the Royal Society*, Vol. 250, April 1958, pp. 411-425.

[17] Sakabe, S. and Izawa, Y., "Simple Formula for the Cross Sections of Resonant Charge Transfer Between Atoms and Their Ions at low Impact Velocity," *Physical Review A*, Vol. 45, No. 3, 1992, pp. 2086-2089.

[18] Birdsall, C.K. and Langdon, A.B., *Plasma Physics Via Computer Simulation*, Adam Hilger Press, 1991.